ACS OMEGA

http://pubs.acs.org/journal/acsodf

Article

Fluorescent Carbon Dots as Biosensor, Green Reductant, and Biomarker

Varsha Raveendran and Renuka Neeroli Kizhakayil*

Cite This: *ACS Omega* 2021, 6, 23475−23484

Read Online

ACCESS | Metrics & More | Article Recommendations

ABSTRACT: Carbon dots, the celebrated green material among the nanocarbon family, are blessed with several interesting features like biocompatibility, solubility, tunable luminescence, and so forth. Herein, carbon dots derived from Mint leaf extract (M-CDs) via a green method are exploited for versatile applications as a biosensor, reductant, and biomarker. M-CDs are applied for fluorimetric sensing of biologically relevant folic acid through quenching response originating from the inner filter effect, with a limit of detection of 280 nM. The carbon dots were highly selective toward folic acid in a collection of 16 biomolecules. The specificity of carbon dots toward folic acid is explained based on the interaction between the two. Along with sensing, herein, we project M-CDs as a green reducing agent by demonstrating the reduction of Fe(III) and noble metal nanoparticle synthesis from their salt solutions. The particles are found to be significantly non-cytotoxic, as evident from the MTT assay performed on primary H8 cells. The application of M-CDs in multicolor imaging is also illustrated using HeLa cells.

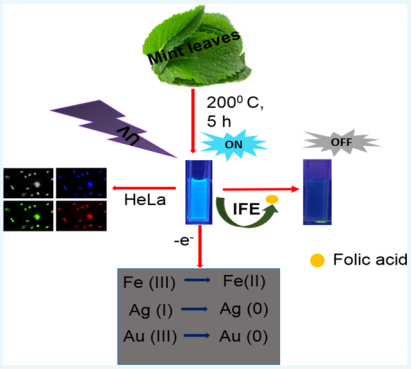

INTRODUCTION

Recently, carbon dots have emerged as a legitimate competitor to the conventional heavy metal-based quantum dots, notably for their potential as a more sustainable and biocompatible alternative.[1−3] These water-soluble, zero-dimensional spherical nanoparticles, having tunable luminescence and photostable nature, have become a promising scaffold in sensing, photocatalysis, biomedical field, etc.[4−12] To date, various chemical and natural precursors have been used to construct carbon dots using various approaches like hydrothermal, solvothermal, arc discharge, pyrolysis, laser ablation, and electrochemical carbonization methods.[2,13] Among these, the green method adopting hydrothermal strategy is an effective one-step bottom-up method, which is widely made use of. Along with this, emphasis is also given for the preparation of carbon dots from natural resources as it benefits from the green and sustainable nature of the precursor moiety. The presence of enormous amounts of cellulose, protein, amino acids, flavanoids, etc. and the added advantages of low cost and easy availability are also claimed by these precursors. The optical properties and biological activities of carbon dots depend on the nature of components and may vary with the choice of the precursor. Accordingly, various biomasses including tomato,[14] potato,[15] banana,[16] lemon,[17] grape juice,[18] mango leaves,[19,20] coriander leaves,[4] neem extract,[21] pomegranate,[22] apple juice,[23] milk,[24] egg,[25] mint leaves,[26] algal blooms,[27] etc. have been explored to this effect.

Mint or *Mentha* (family Lamiaceae) is a widely distributed medicinal herb, which is also used as a flavoring agent. It is well accepted as a remedy for common cold, inflammation, nausea, vomiting, diarrhea, etc.[28] The presence of menthone, piperitone, linalool, camphor, etc. makes Mentha species exhibit antimicrobial, anti-inflammatory, antioxidant, and cytotoxic activities.[29−31] However, the usage of toxic solvents in the extraction procedure limits their biological applications. Like most of the leaf extracts, Mint leaf extract is also examined for the reduction efficiency.[32−34] Although practically effective, the time-consuming extraction procedures make the whole process tedious and the time taken for the reduction process was significantly high. As an excellent alternative with added advantages, we have synthesized Mint leaf-derived carbon dots, which are benefitted not only from reducing nature but also from luminescence-based fine features. Hydrothermal treatment of the leaves under high temperature and pressure leads to dehydration, carbonization, and in situ surface passivation of leaves, which finally leads to the formation of luminescent M-CDs.[4,35,36] Selective detection of folic acid (FA), reduction of metal ions including Fe(III), Ag(I), and Au(III), and cell imaging are effectively enabled by these particles. The role of carbon dots as a reducing agent is less explored compared to other luminescence-based applications of these systems.

Received: July 2, 2021
Accepted: August 17, 2021
Published: August 27, 2021

M-CDs could detect folic acid, also known as vitamin B_9, belonging to the group of water-soluble B group vitamins, with high specificity and sensitivity. FA plays a crucial role in the formation of red blood cells, body growth, and prevention of anemia.[37−39] As a significant biomolecule, the deficiency of FA leads to a number of chronic diseases including stroke, heart attack, psychosis, mentality devolution, neural tube disorder, and so forth, and a high dose may cause pernicious anemia.[40,41] Carbon dots derived from chemical precursors are explored by some researchers to trace this analyte. Li et al. have reported the synthesis of fluorescent carbon dots (CDs) for assaying FA by using citric acid and the ethylene imine polymer as precursors.[42] Aconitic acid and lactose were also utilized in this direction.[41,43] $AgInS_2$ quantum dots were developed by another group for the detection of FA.[44] The practical application of these particles is successfully proved by He et al. through detecting FA in the serum sample by a dual-emission fluorescence nanoprobe.[45] Although some of these systems show considerable sensitivity, none of them provide a proper explanation for the specificity of systems toward FA over other interfering biomolecules. The present system exhibits commendable sensitivity as well as excellent selectivity toward FA in a collection of 16 biomolecules. The limit of detection (LOD) of FA is found to be 280 nM. The specificity of M-CDs toward FA is attributed to the inner filter effect, as evident from a detailed investigation on the mechanism of quenching.[46,47] The highlights of the present work include the usage of a natural precursor to carbon dots, facile green synthesis, excellent selectivity, and more importantly a satisfactory explanation for the selectivity of the system toward FA compared to other analytes.

The performance of these particles as a green reducing agent is also demonstrated along with biosensing. Reduction is one of the most important chemical reactions, which generally involves the usage of toxic chemicals and expensive heavy metals, carried out under harsh reaction conditions. Hitherto, the reducing property of carbon dots is mainly exploited in metal nanoparticle synthesis. M-CDs could successfully reduce Fe^{3+} to Fe^{2+}, where the conversion starts within a few minutes. The one and only precedented work in this direction is by Shariati-Rad et al., who adopted onion and grape CDs for this purpose.[48] The reducing efficiency is further proved through achieving noble metal nanoparticles from the respective metal salts. A noteworthy achievement here is that no heat treatment or addition of other chemical agents is demanded for the reduction process. Silver nanoparticles (AgNPs) are obtained directly within a few minutes in the presence of M-CDs. Jin et al. have used carbon dots derived from a chemical precursor for the synthesis of AgNPs with the aid of heat treatment and other chemical agents.[49] Apart from Ag(I) reduction, M-CDs could yield gold nanoparticles (AuNPs) from Au(III) upon mild heat treatment. Carbon dots serve as both a stabilizing and reducing agent in solution.[50] Finally, by considering the stable and excitation-dependent luminescence nature, the application of M-CDs in multicolor imaging of HeLa (human cervical cancer cell lines) cells has also been demonstrated here.

RESULTS AND DISCUSSION

Characterization of M-CDs. Transmission electron microscopy was used to study the size distribution and morphology of M-CDs.[27,51] As shown in Figure 1a, the dots are of size less than 10 nm. The inset of Figure 1a shows

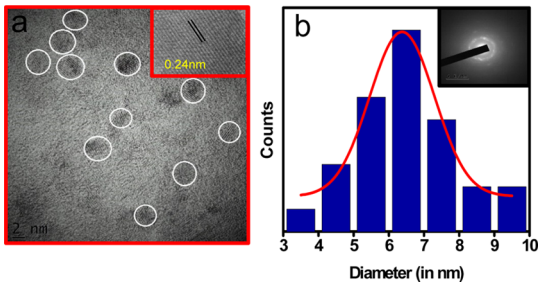

Figure 1. (a) HR-TEM image of M-CDs; the inset shows lattice fringes of M-CDs. (b) Histogram derived from TEM shows particle size distribution. The inset of (b) shows the SAED pattern of M-CDs.

fringes corresponding to the partial crystalline nature of M-CDs.[52] The "*d*" spacing value of 0.24 nm obtained is attributed to the in-plane lattice constant of aromatic carbon or graphene-like structures.[52,53] The size distribution histogram also indicated an average particle size of 6.5 nm (Figure 1b). The selected area electron diffraction (SAED) pattern of M-CDs shown in the inset of Figure 1b confirms their partial crystalline nature.

A single peak in the XRD pattern at 23.58° confirms the graphitic nature with the (002) lattice spacing[54] (Figure 2a). The interlayer spacing value of 0.37 nm, which is greater than that of bulk graphite, indicates a disordered graphitic core. The Raman spectrum of the M-CDs showed two peaks at 1293 and 1603 cm^{-1}, which represent the D band and G band, respectively, corresponding to the vibrations of sp^3 and sp^2 carbon atoms (Figure 2b).[27] The coexistence of the two bands and the intensity ratio (I_D/I_G) of 1.30 also confirm that the prepared CDs possess plenty of structural defects in the core. The surface functional groups of M-CDs were characterized by using FTIR spectroscopy (Figure 2c). The peak around 3439 cm^{-1} could be ascribed to the stretching vibrations of surface −OH groups, whereas the bands at 2918 and 777 cm^{-1} correspond to C−H stretching and bending vibrations, respectively.[4,15,55] The band at 1643 cm^{-1} and the weak one at 1319 cm^{-1} indicate the existence of C═O and C−O stretching vibrations of the carboxylic ester group in the respective data. The results confirm that the M-CDs are functionalized with oxygen-containing groups such as carboxyl, epoxy, and hydroxyl, which originate from the organic groups in Mint leaf extract under hydrothermal reaction conditions.

As depicted in Figure 3a, the bands at 225 and 281 nm in the absorption spectrum of M-CDs correspond to $\pi-\pi^*$ transitions of C═O and C═C bonds, respectively, and the one at 323 nm corresponds to the $n-\pi^*$ transitions of C═O bonds.[36,56,57] An intense photoluminescence (PL) emission was noted at 441 nm at an excitation wavelength of 360 nm (Figure 3b). The M-CD solution shows the brown and cyan colors under daylight and 365 nm UV light, respectively (inset of Figure 3b). The PL decay was recorded at room temperature by using the time-correlated single-photon counting technique. Figure 3c represents the fluorescence decay curve. The average lifetime calculated, τ_{avg} (5.19 ns), suggests that the synthesized M-CDs are suitable for optoelectronic fields as well as biological applications.[58] The quantum yield was found to be 7.64% by using quinine sulfate as the standard.

The successful application of a luminescent material demands high stability.[59] The as-prepared M-CDs show very good fluorescence stability under continuous UV light

https://doi.org/10.1021/acsomega.1c03481
ACS Omega 2021, 6, 23475−23484

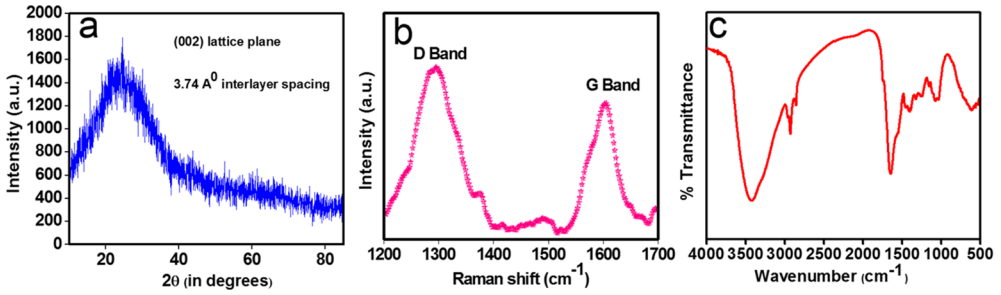

Figure 2. (a) XRD pattern of M-CDs, (b) Raman spectrum of the M-CDs, and (c) FT-IR spectrum of the system.

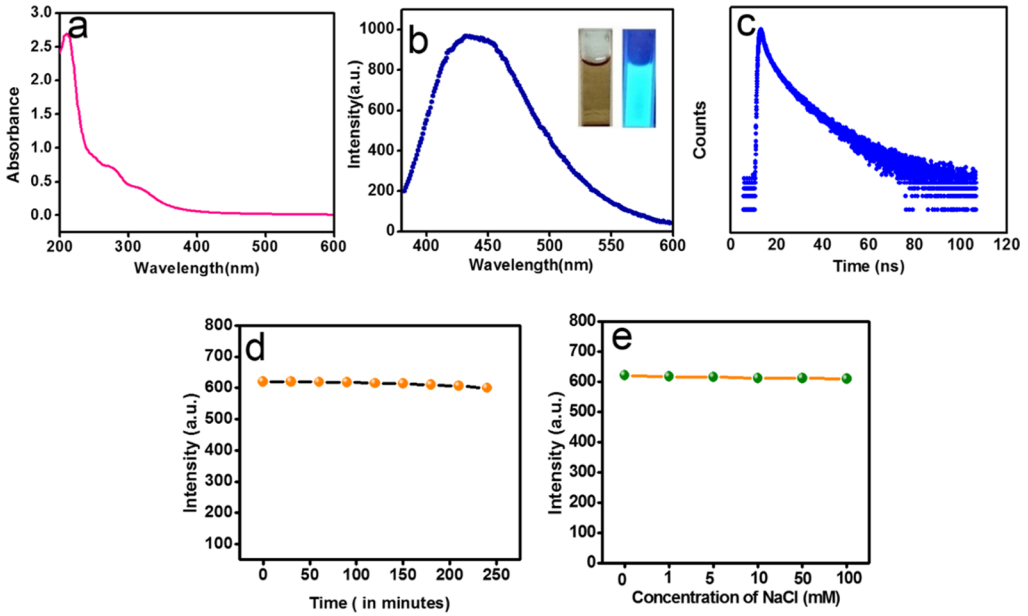

Figure 3. (a) UV−vis spectrum. (b) PL spectrum of the M-CD solution at 360 nm excitation; the inset shows the color of M-CDs in daylight and UV light (365 nm). (c) PL decay curve of M-CDs. The dependence of luminescence intensity of the M-CDs on (d) irradiation time and (e) ionic concentration (NaCl upto 100 mM).

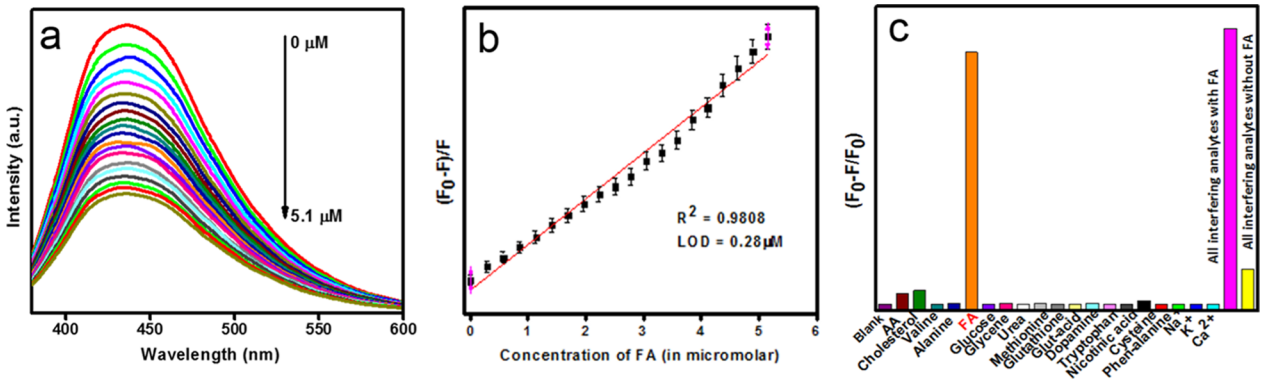

Figure 4. (a) Emission spectrum of M-CDs with increasing amounts of FA; (b) dependence of relative fluorescence quenching efficiency ((F_0 − F)/F) on FA concentration; (c) plot illustrating the selectivity of the system toward FA over other interfering analytes.

irradiation in a UV chamber (365 nm). From Figure 3d, it is clear that fluorescence intensity is almost constant up to 4 h, which assures its efficiency in the fields of bioimaging. In order to examine the stability of M-CDs under high-ionic-strength environments, the PL spectrum of the system in different NaCl concentrations was recorded. The dependence of the fluorescence intensity of the as-prepared M-CDs on ionic strength was estimated in NaCl solutions of different concentrations (0−100 mM). As shown in Figure 3e, the PL intensity is almost the same in the above range of ionic concentrations, indicative of the superior colloidal stability and their application in biological imaging and sensing under more complicated physiological conditions.[60]

Fluorimetric Sensing of FA Using M-CDs. The sensing performance of M-CDs towards various biomolecules was analyzed. As displayed in Figure 4a, the PL intensity at 441 nm

https://doi.org/10.1021/acsomega.1c03481
ACS Omega 2021, 6, 23475−23484

decreased gradually by the introduction of aliquots of folic acid. The fluorescence quenching occurred within a few seconds by the addition of FA. Figure 4b shows the characteristic Stern−Volmer plot between quenching efficiency $((F_0 - F)/F)$ and FA concentration, which shows a good linear relationship (R^2 = 0.9808; F_0 and F are the luminescence intensities of M-CDs in the absence and presence of FA, respectively). The limit of detection (LOD) of the analyte was calculated to be 280 nM. Figure 4 c shows the selectivity of the system toward FA compaired to other biomolecules. A comparison of the performance of other folic acid sensors is summarized in Table 1. It can be seen that the efficiency of M-CDs is definitely considerable when compared to several CDs derived from chemical precursors through complex reaction steps.

Table 1. Comparison of Different Systems in FA Sensing

method	LOD (μM)	refs
citric acid-derived CDs	0.38	42
aconitic acid-derived CDs	0.04	43
CDs from lactose	0.019	41
Ni/POA/CPE	0.28	61
MoS_2 QDs	0.1	62
N-CQDs	0.5×10^{-3}	63
M-CDs	0.28	this work

Selectivity toward Folic acid. Since selectivity is another important feature to be achieved for a sensor, the fluorescence intensity of M-CDs in the presence of various other coexisting biomolecules including cysteine, valine, glycene, phenyl alanine, glucose, urea, dopamine hydrochloride, nicotinic acid, glutathione, glutamic acid, methionine, tryptophan, alanine, cholesterol, and ascorbic acid was examined. As shown in Figure 4c, no significant alteration was noticed in the luminescence intensity of M-CDs in the presence of these afore-mentioned biomolecules, validating the high selectivity of the system toward folic acid (FA). Although there are several other fluorescent sensors for the detection of FA, none of them detail the exact specificity of the system over other biological analytes.[41−43] To deeply probe this matter, the UV absorption spectral behavior of the system toward FA was analyzed. As noted from Figure 5a, a small increase in the absorbance value of M-CDs was observed at 278 nm by the introduction of FA, indicating a special affinity of M-CDs toward FA. According to previous reports, this indicates the formation of FA-functionalized carbon dots.[64] The specificity of the system toward FA is thus expected on the basis of this preliminary observation. However, a more detailed investigation rules out this possibility of functionalization, as illustrated below. First, the absorbance of M-CDs and the specific analyte, FA, and the mixture of M-CDs was recorded using water as the reference. In another set of experiments, the absorbance of the mixture of M-CDs and FA was measured using carbon dot solution as the reference material. On analyzing the spectra in this regard (Figure 5a), it is obvious that the an increase in absorbance of M-CDs around 278 nm observed in the presence of FA accounts for the presence of FA itself in the mixture as the absorbance of the mixture of M-CDs and FA overlaps with that of pure FA in water, in the latter case, with the M-CD solution as the reference. This underlines the absence of complexation or functionalization between the two.

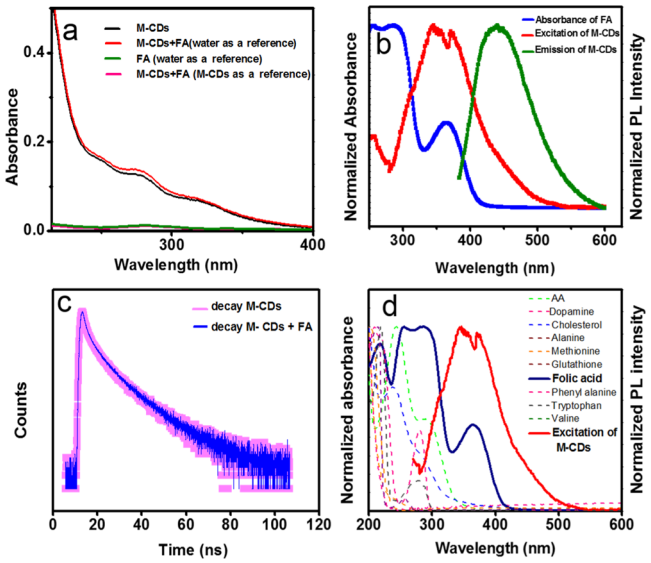

Figure 5. (a) UV absorption spectral behavior of M-CDs alone with water as a reference (black line); the mixture of M-CDs and FA with water as a reference (red line); FA alone with water as a reference (green line); the mixture of M-CDs and FA with M-CDs as a reference (pink line); (b) overlapping of the normalized absorbance spectrum of FA, the excitation spectrum of M-CDs, and the emission spectrum of M-CDs; (c) TCSPC measurements of M-CDs (pink line) and the FA + M-CD mixture (blue line); (d) overlapping of the absorption spectrum of biomolecules and the excitation curve of M-CDs.

Hence, a more lucid explanation strong enough to emphasize the selectivity should be thus formulated. To this effect, optical features of the systems are well examined, probing the mechanism of fluorescence quenching. Fluorescence quenching may occur via various ways such as (i) static quenching and ground-state complex formation between the fluorophore and the analyte, (ii) dynamic quenching, (iii) Forster resonant energy transfer (FRET), (iv) photoinduced electron transfer (PET), the inner filter effect (IFE), and so forth.[65] Therefore, it is imperative to figure out the exact mechanism that leads to the quenching of fluorescence of the M-CDs to remove the ambiguity regarding the selectivity. An analysis to this effect rules out the chance for FRET as there is no overlap between the absorption spectrum of FA and the emission spectrum of M-CDs (Figure 5b). Since FRET- and PET-based electron transfer occurs in the excited state, there should be a substantial change in the fluorescence lifetime of the donor after the introduction of the absorber.[66] To investigate the involvement of FRET, the TCSPC measurements were carried out (Figure 5c). The lifetime values of M-CDs in the absence and presence of FA (1 mM) are 5.19 and 5.41 ns, respectively. A negligible change in the values of lifetime excluded the effect of dynamic quenching and FRET.[67] Another possibility is static quenching. Since static quenching involves the formation of a non-fluorescent ground-state complex, there should be a deflection in the value of absorption maxima of the fluorophore.[66] It was apparent that there was no new peak in the absorption spectrum of the mixed system (Figure 5a), which excluded the participation of the static quenching mechanism in the process. Almost constant lifetime values further substantiate this judgement.

However, as displayed in Figure 5b, there is considerable overlap between the absorption spectrum of FA appearing

https://doi.org/10.1021/acsomega.1c03481
ACS Omega 2021, 6, 23475−23484

around 360 nm and the excitation spectrum of M-CDs. This opened up the chance for the inner filter effect, arising from either the attenuation of the excitation light or absorption of emission radiation by the quencher, to be the causative factor for fluorescence quenching of M-CDs in the presence of FA.[42,67] The trend in the lifetime indicates the absence of chemical reaction between the target analyte and the fluorescent material, which further stresses the occurrence of IFE.[68,69] The conclusion that IFE originates from weakening of excitation of the fluorophore in the presence of FA, as indicated by the overlap of excitation curve of the carbon dot and absorption of FA, provides the explanation of the selectivity pretty well. As seen in Figure 5d, FA alone exhibits a significant overlap with the excitation energy distribution of carbon dots, thus leading to luminescence quenching with high specificity.

The practical application of the as-prepared M-CDs was examined by employing the M-CDs as a fluorescence probe for the detection of FA in FA tablets (Folvite) by the standard addition method. The results are presented in Table 2. The recoveries varied in the range of 98.05−105.42%, which demonstrates the applicability and reliability of FA detection by the M-CD sensor.

Table 2. Real Sample Analysis—FA Content in FA Tablets

spiked (in μM)	found (in μM)	error %	recovery (%)
8.02	7.6	5.2	94.7
16.12	15	6.9	93.05
32.25	34	5.4	105.42
48.38	50	3.3	103.34
64.5	65.9	2.7	102.7

M-CDs as a Reducing Agent. *Reduction of Fe^{3+} to Fe^{2+}.* The reducing ability of the as-synthesized M-CDs is demonstrated through the reduction of Fe^{3+} to Fe^{2+}. A color change was noted in Fe^{3+} solution to pale green upon the addition of CDs, concomitant with the appearance of a broad peak around the 500−700 nm region in the UV absorbance spectrum (Figure 6a). Such an observation confirms the reducing nature of carbon dots. The formation of Fe^{2+} was further proven by taking 1,10 phenanthroline as the complexating agent for ferrous ions. Figure 6b shows the spectra of a mixture of Fe^{3+} and 1,10 phenanthroline in presence and absence of M-CDs. In the presence of carbon dots, an additional peak around 500 nm was observed, and the same was absent in the mixture of the former two species. The above-mentioned peak signifies complexation between Fe^{2+} and 1,10 phenanthroline, indicated by the color change to orange (inset of Figure 6 b). This observation confirms the reducing ability of the prepared M-CDs, a property attributed to the surface hydroxyl groups present on carbon dots.[48]

To study the effect of time in the reduction reaction, absorption spectra of the mixture of M-CDs (200 μL), ferric chloride (1.5 mL, 1 mM), and 1,10 phenanthroline (100 μL, 9 mM) at different time intervals were recorded. Figure 6c displays the UV−visible spectra of the mixture of Fe(III), 1,10 phenanthroline and M-CDs in 1−10 min. An intense peak around 500 nm was observed within 1 min after the addition of M-CDs to the Fe(III) and 1,10 phenanthroline mixture. The absorbance increases and becomes stable in 5−10 min, and no noticeable change occurs after that, which implies the completion of reduction of Fe^{3+} within 10 min. The inset of Figure 6c agrees with this observation.

Synthesis of Silver and Gold nanoparticles. The reducing nature of the as-synthesized M-CD is further demonstrated through the formation of silver and gold nanoparticles (AgNPs and AuNPs) from the respective salt solutions. Addition of CDs to Ag(I) solution affected Ag(0) formation in the absence of any stabilizing agent and heat treatment, as indicated by the color change of Ag(I) solution to brownish yellow. The observation was noted within 10 min following the addition of M-CDs to 1 mM $AgNO_3$ solution. The formation of the particles in the nanoregime is confirmed by the surface plasmon resonance (SPR) peak at 438 nm. As nanoparticle synthesis is proven to be a time-dependent process, the absorption spectra at different time intervals were recorded to investigate the reaction process. Figure 7a displays the UV−visible spectra of the reaction mixture in 24 h. The formation of AgNPs occurred in just 10 min, and a gradual increase in intensity of the peaks at the same intensity maxima confirms that the time elapse has not influenced the silver particle size. The inset of Figure 7a shows the synthesized silver nanoparticle solution by the addition of M-CDs. The average particle size determined from the HRTEM image is found to be around 12 nm (Figure 7b). The lattice fringes shown in the inset of Figure 7b and the SAED pattern presented in Figure 7c clearly reveal the crystallinity of metal nanoparticles.

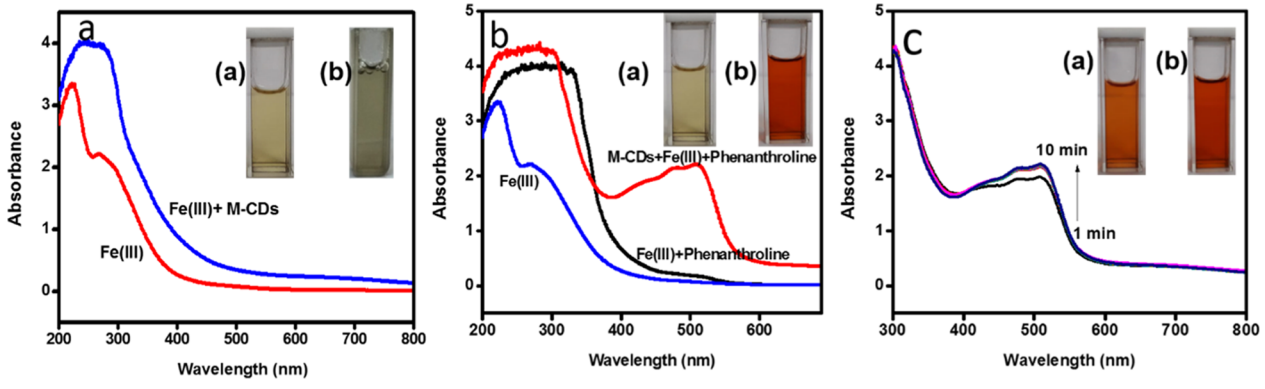

Figure 6. (a) Absorption spectrum of Fe^{3+} (red line) and Fe^{3+} plus M-CDs (blue line); the inset shows the photographic image of (a) Fe^{3+} solution (b) Fe^{3+} in the presence of M-CDs. (b) UV−visible spectrum of Fe^{3+}(blue line), Fe^{3+} plus phenanthroline (black line), and (c) Fe^{3+} plus 1,10 phenanthroline in the presence of M-CDs; the insets show the corresponding photographic images. (c) Absorption spectra of Fe^{3+} plus 1,10 phenanthroline in 1−10 min in the presence of M-CDs. The images of intensity variations are shown in the inset.

https://doi.org/10.1021/acsomega.1c03481
ACS Omega 2021, 6, 23475−23484

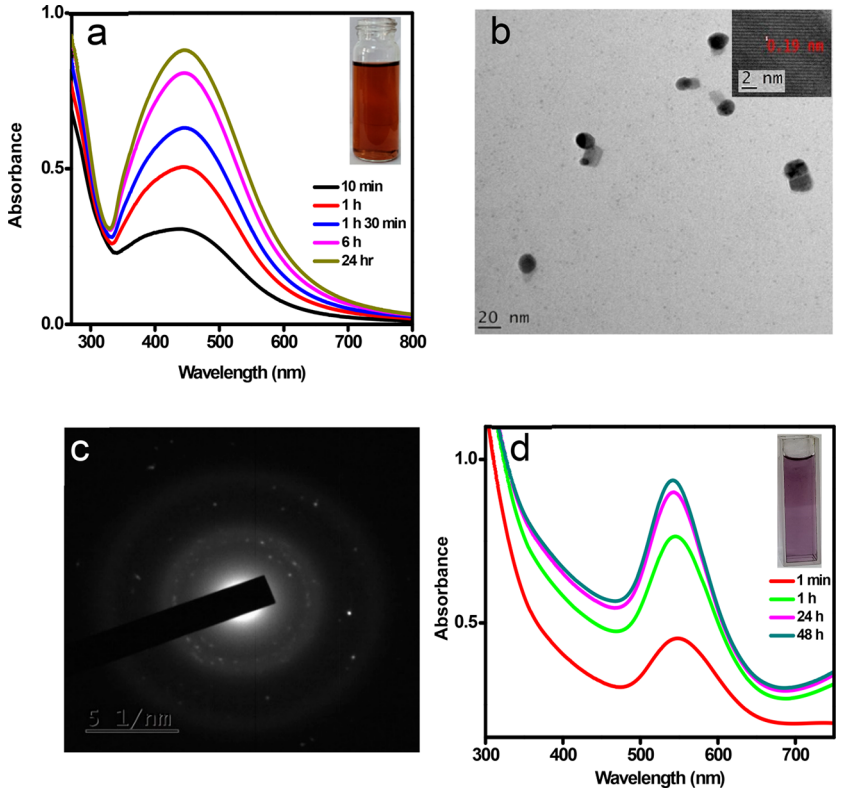

Figure 7. (a) Absorption spectra of AgNPs synthesized (b) HRTEM image of AgNPs, inset shows the lattice fringes at higher magnification. (c) SAED pattern of AgNPs obtained from TEM. (d) Absorption spectra of gold nanoparticles synthesized by using M-CDs as reducing agent.

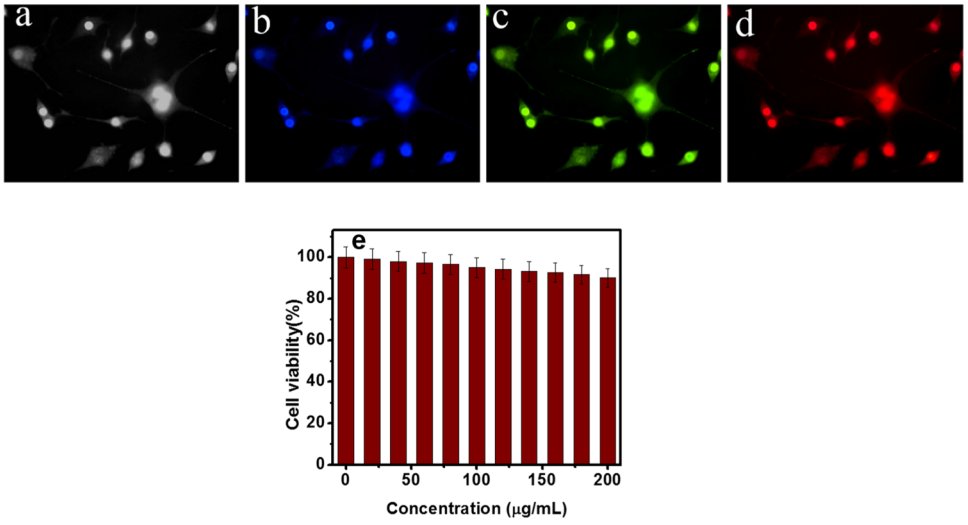

Figure 8. Fluorescence microscopy image of HeLa cells, control (a) and under excitation wavelengths of 360−380 nm (b), 460−480 nm (c), and 510−590 nm (d). Percentage cell viability of primary H8 cells in the presence of M-CDs of varying concentrations (e).

AuNPs were achieved by mild heat treatment of Au(III) solution with CDs in the presence of small quantities of starch solution as a capping agent. The pale-yellow solution of $HAuCl_4$ turned to purple in 5 min, which indicates the formation of AuNPs. The UV−visible spectrum shown in Figure 7d substantiates the nanoparticle formation, where the SPR band appeared at 540 nm. The absorption maxima at this position suggest an average particle size of 60 nm to the as-prepared AuNPs. The time-dependent absorption spectral maxima reveal that the formed particles are considerably stable.

HeLa Cell Imaging. Considering the strong and stable PL of the M-CDs, it becomes worthwhile to check whether the present system can be utilized for fluorescence imaging of cells. The fluorescence images of M-CD-treated HeLa cells were recorded to this effect. The hydrophilic nature and the presence of functional groups on the surface of M-CDs enable effortless internalization of them into the cells via endocytosis.[23] The cell images excited with long-wavelength UV light (360−380 nm), blue light (460−480 nm), and green light (510−590 nm) are displayed in Figure 8. Successful application of M-CDs as an effective probe for imaging is

https://doi.org/10.1021/acsomega.1c03481
ACS Omega 2021, 6, 23475−23484

assured through these results. MTT assay was conducted to check the biocompatible nature of the present system by taking primary H8 cells as the model. The percentage cell viability results illustrated in Figure 8e reveal no significant cytotoxicity of M-CDs (0−200 μg/mL) on normal H8 cells, thus ensuring the safe use of the system for biological applications like cell imaging.

CONCLUSIONS

In summary, a simple and green route for the synthesis of cyan luminescent carbon dots from Mint leaves is developed without any surface modification. The intrinsic fluorescence of M-CDs could be quenched in the presense of FA through the inner filter effect, enabling the fabrication of a fluorescent sensor for the former. The as-prepared M-CDs were highly stable under continuous UV light irradiation and were stable over a wide range of ionic concentrations. The synthesized M-CDs could be used as an effective green reducing agent for ferric ion reduction as well as for the production of stable silver and gold nanoparticles. The M-CDs were found to be significantly non-cytotoxic towards primary H8 cells, as evident from the MTT assay. The strong and excitation-dependent emission of the system made it an excellent candidate in the multicolor imaging of HeLa cells.

EXPERIMENTAL SECTION

Materials. Fresh mint leaves were obtained from a local market and were washed thoroughly before use. Quinine sulfate, sodium chloride, sodium hydroxide, 1,10 phenanthroline, and hydrochloric acid were supplied by Merck Ltd., India. L-Ascorbic acid, glutamic acid, glutathione, FA, valin, phenyl alanine, alanine, nicotinic acid, glycine, cysteine, glucose, urea, dopamine hydrochloride, cholesterol, tryptophan, silver nitrate, trichlorogold hydrochloride, etc. were purchased from Sigma-Aldrich.The human cervical cancer cell line (HeLa) and primary H8 cells were obtained from the National Center for Cell Science (NCCS, Pune), and MTT was purchased from Sigma-Aldrich (Bangalore). Dulbecco's modified Eagle's medium (DMEM) and fetal bovine serum polybrene analytical grade reagents were purchased from Sigma-Aldrich (Bangalore). DMSO, paraformaldehyde, the antibiotic−antimycotic (1%), L-glutamine, and *p*-nitroanilide were purchased from Sigma-Aldrich. All the samples were prepared in Milli-Q water.

Synthesis of CDs. The synthesis of CDs is similar to that of our previous work.[26] Briefly, 5 g of the fresh mint leaves was washed well with deionized water, chopped, and crushed in a mortar. It was dissolved in 40 mL of deionized water and stirred for 30 min. The extract then underwent hydrothermal treatment at 200 °C for 5 h. Then, the insoluble portion was filtered off and subjected to centrifugation at 2500 rpm for 1 h. The brown-colored M-CD solution obtained was then stored in 4 °C for further characterizations and studies.

Characterizations of M-CDs. The absorbance and fluorescence spectra of the M-CDs were recorded by using a JASCO V-550 spectrophotometer and Cary Eclipse (Agilent Technology) fluorescence spectrophotometer, respectively. An LZC-4X photoreactor was used for measuring of the luminescence nature of the prepared sample. The X-ray diffraction (XRD) pattern of the sample was recorded using a RigakuMiniflex-II diffractometer using Cu Kα radiation in the scan range of 2θ 20−80°. The morphology and the particle size were obtained by transmission electron microscopy (JEOL JEM 2100). The sample for TEM analysis was prepared by dropping an aqueous solution of carbon dots on the copper grid coated with carbon. Fourier transmission infrared (FTIR) spectra were recorded using a JASCO FTIR-4100 instrument using the KBr disc method. The Raman spectrum was recorded using a LabRam HR-Horiba Jobinyvon Spectrometer using a Raman Microprobe with a 532 nm Nd:YAG excitation source. A fluorescence microscope (Nikon Eclipse, Inc., Japan) at 40× magnification was employed for the imaging of HeLa cells incubated with CDs.

FA Sensing. 100 μM stock solutions of biomolecules including ascorbic acid, nicotinic acid, FA, glysene, cysteine, glutamic acid, valin, phenyl alanine, methionine, dopamine hydrochloride, tryptophan, cholesterol, alanine, and glutathione were prepared. 3.5 mL of the M-CD solution was taken in a cuvette, and different concentrations of the analyte solutions were added. Then, the solution was kept for a few seconds, and then, the aliquots were subjected for the fluorescence assay at an excitation wavelength of 360 nm. In order to advocate the practical applicability of the sensor, FA detection in tablets (Folvite) was carried out.

Reduction of Fe^{3+} to Fe^{2+}. The reduction of ferric to ferrous ions was carried out simply by using the synthesized M-CD solution. The yellow color of ferric chloride solution changed to a pale-green color immediately after the addition of the prepared carbon dot solution. The formation of Fe(II) from Fe(III) was conformed by 1,10 phenanthroline as the complexing agent. In a typical procedure, 1.5 mL of iron(III) chloride solution (1 mM) was mixed with 100 μL of 1,10 phenanthroline(10 mM). Subsequently, 200 μL of the M-CD solution was added to this mixture, and the color change was noted. The absorbance of the solution was recorded using a UV−visible spectrophotometer.

Synthesis of Silver Nanoparticles. The procedure for preparing AgNPs by M-CDs as both a reductant and stabilising agent is as follows: 250 μL of M-CDs was added to 20 mL of silver nitrate solution (1 mM) taken in a glass bottle. After 10 min, the color of the solution (silver nitrate + M-CDs) changed from colorless to yellowish brown, indicating the formation of silver nanoparticles. The formation and growth of the nanoparticles were monitored using a UV−visible spectrophotometer.

AuNP Synthesis. AuNPs were prepared by reacting tetrachloroaurate ($HAuCl_4$) with M-CDs as the reducing agent and starch as the stabilizer. Briefly, 50 μL of $HAuCl_4$ solution (0.05 M) was added to 20 mL of water taken in a beaker. The solution was heated to 60 °C for 1 min, followed by the addition of 500 μL of M-CDs and a very small quantity of 1% starch solution with constant stirring. The color of the gold solution changed to purple, indicating the formation of AuNPs, which is monitored through the UV−visible spectrophotometer.

Evaluation of Cytotoxicity (MTT Assay). The inhibitory concentration (IC_{50}) value was evaluated using an MTT assay. The primary H8 cells were grown (1×10^4 cells/well) in a 96-well plate for 48 h in to 75% confluence. The medium was replaced with a fresh medium containing synthesized compounds, and the cells were further incubated for 48 h. The culture medium was removed, and 100 μL of the MTT (Hi-Media) solution was added to each well and incubated at 37 °C for 4 h. 50 μL of DMSO was added to each of the wells after the removal of the supernatant and incubated for 10 min to solubilize the formazan crystals. In an ELISA multiwell plate

https://doi.org/10.1021/acsomega.1c03481
ACS Omega 2021, 6, 23475−23484

reader (Thermo Multiskan EX, USA), the optical density (OD) was measured. The OD value was used to calculate the percentage of viability of cells using the formula % of viability = (OD value of the experimental sample/OD value of the experimental control) × 100.

Cell Incubation and Imaging. Human cervical cancer HeLa cells were maintained in DMEM supplemented with FBS (10%), L-glutamine (2 mM), the antibiotic−antimycotic (1%), and non-essential amino acids (1%) in 5% CO_2 at 37 °C. Then, the cells were seeded in 96-well plates at a cell density of 1×10^4 cells per mL. 100 μL of the mixture of M-CDs and polybrene were added to each well, which was incubated for 24 h. The precipitated cells were washed thrice with PBS before being used for bright-field and PL imaging measurements using a fluorescence microscope (Nikon Eclipse, Inc., Japan) at 40× magnification. The excitation wavelengths were set in the ranges of 510−590, 460−480 and 360−380 nm.

AUTHOR INFORMATION

Corresponding Author

Renuka Neeroli Kizhakayil − *Department of Chemistry, University of Calicut, Malappuram, Kerala 673 635, India;* orcid.org/0000-0001-6333-5316; Phone: +914942407413; Email: nkrenu@gmail.com; Fax: +914942400269

Author

Varsha Raveendran − *Department of Chemistry, University of Calicut, Malappuram, Kerala 673 635, India*

Complete contact information is available at: https://pubs.acs.org/10.1021/acsomega.1c03481

Notes

The authors declare no competing financial interest.

ACKNOWLEDGMENTS

V.R. P.T acknowledges KSCSTE (Kerala State Council for Science, Technology and Environment) for their financial support. The authors thank CSIF, University of Calicut, for the analytical methods. The authors also thank Dr. Vimala K, Division of Cancer Nanomedicine, Department of Zoology, Periyar University, Salem, Tamilnadu, for the help rendered in biomedical studies using carbon dots.

REFERENCES

(1) Wang, R.; Lu, K.-Q.; Tang, Z.-R.; Xu, Y.-J. Recent progress in carbon quantum dots: synthesis, properties and applications in photocatalysis. *J. Mater. Chem. A* **2017**, *5*, 3717−3734.

(2) Wang, Y.; Hu, A. Carbon quantum dots: synthesis, properties and applications. *J. Mater. Chem. C* **2014**, *2*, 6921−6939.

(3) Feng, X.; Jiang, K.; Zeng, H.; Lin, H. A Facile Approach to Solid-State White Emissive Carbon Dots and Their Application in UV-Excitable and Single-Component-Based White LEDs. *Nanomaterials* **2019**, *9*, 725.

(4) Sachdev, A.; Gopinath, P. Green synthesis of multifunctional carbon dots from coriander leaves and their potential application as antioxidants, sensors and bioimaging agents. *Analyst* **2015**, *140*, 4260−4269.

(5) Bartelmess, J.; Quinn, S. J.; Giordani, S. Carbon nanomaterials: multi-functional agents for biomedical fluorescence and Raman imaging. *Chem. Soc. Rev.* **2015**, *44*, 4672−4698.

(6) Gao, X.; Du, C.; Zhuang, Z.; Chen, W. Carbon quantum dot-based nanoprobes for metal ion detection. *J. Mater. Chem. C* **2016**, *4*, 6927−6945.

(7) Zhuo, S.; Guan, Y.; Li, H.; Fang, J.; Zhang, P.; Du, J.; Zhu, C. Facile fabrication of fluorescent Fe-doped carbon quantum dots for dopamine sensing and bioimaging application. *Analyst* **2019**, *144*, 656−662.

(8) Wang, C.; Shi, H.; Yang, M.; Yan, Y.; Liu, E.; Ji, Z.; Fan, J. Facile synthesis of novel carbon quantum dots from biomass waste for highly sensitive detection of iron ions. *Mater. Res. Bull.* **2020**, *124*, 110730.

(9) Pirsaheb, M.; Asadi, A.; Sillanpää, M.; Farhadian, N. Application of carbon quantum dots to increase the activity of conventional photocatalysts: A systematic review. *J. Mol. Liq.* **2018**, *271*, 857−871.

(10) Ke, J.; Li, X.; Zhao, Q.; Liu, B.; Liu, S.; Wang, S. Upconversion carbon quantum dots as visible light responsive component for efficient enhancement of photocatalytic performance. *J. Colloid Interface Sci.* **2017**, *496*, 425−433.

(11) Lin, F.; Bao, Y.-W.; Wu, F.-G. Carbon dots for sensing and killing microorganisms. *C* **2019**, *5*, 33.

(12) Chakraborty, D.; Sarkar, S.; Das, P. K. Blood dots: hemoglobin-derived carbon dots as hydrogen peroxide sensors and pro-drug activators. *ACS Sustainable Chem. Eng.* **2018**, *6*, 4661−4670.

(13) Dimos, K. Carbon quantum dots: surface passivation and functionalization. *Curr. Org. Chem.* **2016**, *20*, 682−695.

(14) Kailasa, S. K.; Ha, S.; Baek, S. H.; Phan, L. M. T.; Kim, S.; Kwak, K.; Park, T. J. Tuning of carbon dots emission color for sensing of Fe3+ ion and bioimaging applications. *Mater. Sci. Eng., C* **2019**, *98*, 834−842.

(15) Mehta, V. N.; Jha, S.; Singhal, R. K.; Kailasa, S. K. Preparation of multicolor emitting carbon dots for HeLa cell imaging. *New J. Chem.* **2014**, *38*, 6152−6160.

(16) Atchudan, R.; Jebakumar Immanuel Edison, T. N.; Shanmugam, M.; Perumal, S.; Somanathan, T.; Lee, Y. R. Sustainable synthesis of carbon quantum dots from banana peel waste using hydrothermal process for in vivo bioimaging. *Phys. E* **2021**, *126*, 114417.

(17) Ding, H.; Zhou, X.; Qin, B.; Zhou, Z.; Zhao, Y. Highly fluorescent near-infrared emitting carbon dots derived from lemon juice and its bioimaging application. *J. Lumin.* **2019**, *211*, 298−304.

(18) Ahmadian-Fard-Fini, S.; Salavati-Niasari, M.; Ghanbari, D. Hydrothermal green synthesis of magnetic Fe3O4-carbon dots by lemon and grape fruit extracts and as a photoluminescence sensor for detecting of E. coli bacteria. *Spectrochim. Acta, Part A* **2018**, *203*, 481−493.

(19) Singh, J.; Kaur, S.; Lee, J.; Mehta, A.; Kumar, S.; Kim, K.-H.; Basu, S.; Rawat, M. Highly fluorescent carbon dots derived from Mangifera indica leaves for selective detection of metal ions. *Sci. Total Environ.* **2020**, *720*, 137604.

(20) Kumawat, M. K.; Thakur, M.; Gurung, R. B.; Srivastava, R. Graphene quantum dots from mangifera indica: application in near-infrared bioimaging and intracellular nanothermometry. *ACS Sustainable Chem. Eng.* **2017**, *5*, 1382−1391.

(21) Roy, P.; Periasamy, A. P.; Chuang, C.; Liou, Y.-R.; Chen, Y.-F.; Joly, J.; Liang, C.-T.; Chang, H.-T. Plant leaf-derived graphene quantum dots and applications for white LEDs. *New J. Chem.* **2014**, *38*, 4946−4951.

(22) Akhgari, F.; Samadi, N.; Farhadi, K. Fluorescent carbon dot as nanosensor for sensitive and selective detection of cefixime based on inner filter effect. *J. Fluoresc.* **2017**, *27*, 921−927.

(23) Mehta, V. N.; Jha, S.; Basu, H.; Singhal, R. K.; Kailasa, S. K. One-step hydrothermal approach to fabricate carbon dots from apple juice for imaging of mycobacterium and fungal cells. *Sens. Actuators, B* **2015**, *213*, 434−443.

(24) Wang, L.; Zhou, H. S. Green synthesis of luminescent nitrogen-doped carbon dots from milk and its imaging application. *Anal. Chem.* **2014**, *86*, 8902−8905.

(25) Zhao, Y.; Zhang, Y.; Liu, X.; Kong, H.; Wang, Y.; Qin, G.; Cao, P.; Song, X.; Yan, X.; Wang, Q.; Qu, H. Novel carbon quantum dots from egg yolk oil and their haemostatic effects. *Sci. Rep.* **2017**, *7*, 1−8.

(26) Raveendran, V.; Suresh Babu, A. R.; Renuka, N. K. Mint leaf derived carbon dots for dual analyte detection of Fe (iii) and ascorbic acid. *RSC Adv.* **2019**, *9*, 12070−12077.

(27) Ramanan, V.; Thiyagarajan, S. K.; Raji, K.; Suresh, R.; Sekar, R.; Ramamurthy, P. Outright green synthesis of fluorescent carbon dots from eutrophic algal blooms for in vitro imaging. *ACS Sustainable Chem. Eng.* **2016**, *4*, 4724−4731.
(28) Jain, D.; Pathak, N.; Khan, S.; Raghuram, G. V.; Bhargava, A.; Samarth, R.; Mishra, P. K. Evaluation of cytotoxicity and anticarcinogenic potential of Mentha leaf extracts. *Internet J. Toxicol.* **2011**, *30*, 225−236.
(29) Hussain, A. I.; Anwar, F.; Nigam, P. S.; Ashraf, M.; Gilani, A. H. Seasonal variation in content, chemical composition and antimicrobial and cytotoxic activities of essential oils from four Mentha species. *J. Sci. Food Agric.* **2010**, *90*, 1827−1836.
(30) Gulluce, M.; Sahin, F.; Sokmen, M.; Ozer, H.; Daferera, D.; Sokmen, A.; Polissiou, M.; Adiguzel, A.; Ozkan, H. Antimicrobial and antioxidant properties of the essential oils and methanol extract from Mentha longifolia L. ssp. longifolia. *Food Chem.* **2007**, *103*, 1449−1456.
(31) Pandey, A. K.; Rai, M. K.; Acharya, D. Chemical composition and antimycotic activity of the essential oils of corn mint (Mentha arvensis) and lemon grass (Cymbopogon flexuosus) against human pathogenic fungi. *Pharm. Biol.* **2003**, *41*, 421−425.
(32) Bhoir, S. A.; Chawla, S. P. Silver nanoparticles synthesized using mint extract and their application in chitosan/gelatin composite packaging film. *Int. J. Nanosci.* **2017**, *16*, 1650022.
(33) Babu, P. J.; Sharma, P.; Borthakur, B. B.; Das, R. K.; Nahar, P.; Bora, U. Synthesis of gold nanoparticles using Mentha arvensis leaf extract. *Int. J. Green Nanotechnol.: Phys. Chem.* **2010**, *2*, P62−P68.
(34) Brown, N.; John, J. A.; Shahidi, F. Polyphenol composition and antioxidant potential of mint leaves. *Food Prod. Process Nutr.* **2019**, *1*, 1−14.
(35) Huang, H.; Xu, Y.; Tang, C.-J.; Chen, J.-R.; Wang, A.-J.; Feng, J.-J. Facile and green synthesis of photoluminescent carbon nanoparticles for cellular imaging. *New J. Chem.* **2014**, *38*, 784−789.
(36) Park, S. Y.; Lee, H. U.; Park, E. S.; Lee, S. C.; Lee, J.-W.; Jeong, S. W.; Kim, C. H.; Lee, Y.-C.; Huh, Y. S.; Lee, J. Photoluminescent green carbon nanodots from food-waste-derived sources: large-scale synthesis, properties, and biomedical applications. *ACS Appl. Mater. Interfaces* **2014**, *6*, 3365−3370.
(37) Tepeli Büyüksünetci, Y.; Haklı, Ö.; Anik, Ü. Centri-Voltammetric Folic Acid Detection. *Electroanalysis* **2020**, *32*, 470−478.
(38) Akbar, S.; Anwar, A.; Kanwal, Q. Electrochemical determination of folic acid: A short review. *Anal. Biochem.* **2016**, *510*, 98−105.
(39) Liu, Y.; Shen, J.; Yang, X.; Sun, Q.; Yang, X. Folic acid reduced triglycerides deposition in primary chicken hepatocytes. *J. Sci. Food Agric.* **2018**, *66*, 13162−13172.
(40) Dai, H.; Li, Y.; Zhang, S.; Gong, L.; Li, X.; Lin, Y. Delicate photoelectrochemical sensor for folic acid based on carbon nanohorns supported interwoven titanate nanotubes. *Sens. Actuators, B* **2016**, *222*, 120−126.
(41) Chen, Z.; Wang, J.; Miao, H.; Wang, L.; Wu, S.; Yang, X. Fluorescent carbon dots derived from lactose for assaying folic acid. *Sci. China: Chem.* **2016**, *59*, 487−492.
(42) Li, W.; Zhang, X.; Miao, C.; Li, R.; Ji, Y. Fluorescent paper−based sensor based on carbon dots for detection of folic acid. *Anal. Bioanal. Chem.* **2020**, *412*, 2805−2813.
(43) Qian, J.; Quan, F.; Zhao, F.; Wu, C.; Wang, Z.; Zhou, L. Aconitic acid derived carbon dots: Conjugated interaction for the detection of folic acid and fluorescence targeted imaging of folate receptor overexpressed cancer cells. *Sens. Actuators, B* **2018**, *262*, 444−451.
(44) Tu, Y.; Chen, X.; Xiang, Y.; Yuan, X.; Qin, K.; Wei, Y.; Xu, Z.; Zhang, Q.; Ji, X. Hydrothermal Synthesis of a Novel Mesoporous Silica Fluorescence Carbon Dots and Application in Cr (VI) and Folic Acid Detection. *NANO* **2020**, *15*, 2050090.
(45) He, Y.; Wang, S.; Wang, J. Detection and quantification of folic acid in serum via a dual-emission fluorescence nanoprobe. *Anal. Bioanal. Chem.* **2019**, *411*, 7481−7487.
(46) Han, L.; Liu, S. G.; Liang, J. Y.; Ju, Y. J.; Li, N. B.; Luo, H. Q. pH-mediated reversible fluorescence nanoswitch based on inner filter effect induced fluorescence quenching for selective and visual detection of 4-nitrophenol. *J. Hazard. Mater.* **2019**, *362*, 45−52.
(47) Jiang, H.; Zhang, W.; Li, J.; Nie, L.; Wu, K.; Duan, H.; Xiong, Y. Inner-filter effect based fluorescence-quenching immunochromotographic assay for sensitive detection of aflatoxin B1 in soybean sauce. *Food Control* **2018**, *94*, 71−76.
(48) Shariati-Rad, M.; Mohseninasab, T.; Parno, F. Application of response surface methodology and green carbon dots as reducing agents in speciation of iron. *RSC Adv.* **2018**, *8*, 2173−2180.
(49) Jin, J.-C.; Xu, Z.-Q.; Dong, P.; Lai, L.; Lan, J.-Y.; Jiang, F.-L.; Liu, Y. One-step synthesis of silver nanoparticles using carbon dots as reducing and stabilizing agents and their antibacterial mechanisms. *Carbon* **2015**, *94*, 129−141.
(50) Ndikau, M.; Noah, N. M.; Andala, D. M.; Masika, E. Green synthesis and characterization of silver nanoparticles using Citrullus lanatus fruit rind extract. *Int. J. Anal. Chem.* **2017**, *2017*, 8108504.
(51) Chao, D.; Lyu, W.; Liu, Y.; Zhou, L.; Zhang, Q.; Deng, R.; Zhang, H. Solvent-dependent carbon dots and their applications in the detection of water in organic solvents. *J. Mater. Chem. C* **2018**, *6*, 7527−7532.
(52) John, J.; Mathew, R. M.; Thomas, T.; Abraham, R.; Rejeena, I.; Jayakrishnan, R.; Chacko, F.; Thomas, V. Tunable light emission using crystalline carbon dots. *J. Opt.* **2019**, *48*, 288−293.
(53) Fu, M.; Ehrat, F.; Wang, Y.; Milowska, K. Z.; Reckmeier, C.; Rogach, A. L.; Stolarczyk, J. K.; Urban, A. S.; Feldmann, J. Carbon dots: a unique fluorescent cocktail of polycyclic aromatic hydrocarbons. *Nano Lett.* **2015**, *15*, 6030−6035.
(54) Vandarkuzhali, S. A. A.; Natarajan, S.; Jeyabalan, S.; Sivaraman, G.; Singaravadivel, S.; Muthusubramanian, S.; Viswanathan, B. Pineapple peel-derived carbon dots: applications as sensor, molecular keypad lock, and memory device. *ACS Omega* **2018**, *3*, 12584−12592.
(55) Alam, A.-M.; Park, B.-Y.; Ghouri, Z. K.; Park, M.; Kim, H.-Y. Synthesis of carbon quantum dots from cabbage with down-and up-conversion photoluminescence properties: excellent imaging agent for biomedical applications. *Green Chem.* **2015**, *17*, 3791−3797.
(56) Zhang, X.; Wang, S.; Zhu, C.; Liu, M.; Ji, Y.; Feng, L.; Tao, L.; Wei, Y. Carbon-dots derived from nanodiamond: Photoluminescence tunable nanoparticles for cell imaging. *J. Colloid Interface Sci.* **2013**, *397*, 39−44.
(57) Lu, Y.-C.; Chen, J.; Wang, A.-J.; Bao, N.; Feng, J.-J.; Wang, W.; Shao, L. Facile synthesis of oxygen and sulfur co-doped graphitic carbon nitride fluorescent quantum dots and their application for mercury (II) detection and bioimaging. *J. Mater. Chem. C* **2015**, *3*, 73−78.
(58) Vikneswaran, R.; Ramesh, S.; Yahya, R. Green synthesized carbon nanodots as a fluorescent probe for selective and sensitive detection of iron (III) ions. *Mater. Lett.* **2014**, *136*, 179−182.
(59) Li, Y.; Bai, G.; Zeng, S.; Hao, J. Theranostic carbon dots with innovative NIR-II emission for in vivo renal-excreted optical imaging and photothermal therapy. *ACS Appl. Mater. Interfaces* **2019**, *11*, 4737−4744.
(60) Wu, F.; Su, H.; Wang, K.; Wong, W.-K.; Zhu, X. Facile synthesis of N-rich carbon quantum dots from porphyrins as efficient probes for bioimaging and biosensing in living cells. *Int. J. Nanomed.* **2017**, *12*, 7375.
(61) Ojani, R.; Raoof, J.-B.; Zamani, S. Electrocatalytic Oxidation of Folic Acid on Carbon Paste Electrode Modified by Nickel Ions Dispersed into Poly (o-anisidine) Film. *Electroanalysis* **2009**, *21*, 2634−2639.
(62) Peng, Y.; Dong, W.; Wan, L.; Quan, X. Determination of folic acid via its quenching effect on the fluorescence of MoS 2 quantum dots. *Microchim. Acta* **2019**, *186*, 605.
(63) Wang, M.; Jiao, Y.; Cheng, C.; Hua, J.; Yang, Y. Nitrogen-doped carbon quantum dots as a fluorescence probe combined with magnetic solid-phase extraction purification for analysis of folic acid in human serum. *Anal. Bioanal. Chem.* **2017**, *409*, 7063−7075.

https://doi.org/10.1021/acsomega.1c03481
ACS Omega 2021, 6, 23475−23484

(64) Zhao, X.; Zhang, J.; Shi, L.; Xian, M.; Dong, C.; Shuang, S. Folic acid-conjugated carbon dots as green fluorescent probes based on cellular targeting imaging for recognizing cancer cells. *RSC Adv.* **2017**, *7*, 42159−42167.
(65) Sun, J.; Zhao, J.; Wang, L.; Li, H.; Yang, F.; Yang, X. Inner filter effect-based sensor for horseradish peroxidase and its application to fluorescence immunoassay. *ACS Sens.* **2018**, *3*, 183−190.
(66) Zu, F.; Yan, F.; Bai, Z.; Xu, J.; Wang, Y.; Huang, Y.; Zhou, X. The quenching of the fluorescence of carbon dots: a review on mechanisms and applications. *Microchim. Acta* **2017**, *184*, 1899−1914.
(67) Tanwar, A. S.; Patidar, S.; Ahirwar, S.; Dehingia, S.; Iyer, P. K. "Receptor free" inner filter effect based universal sensors for nitroexplosive picric acid using two polyfluorene derivatives in the solution and solid states. *Analyst* **2019**, *144*, 669−676.
(68) Lin, L.; Rong, M.; Lu, S.; Song, X.; Zhong, Y.; Yan, J.; Wang, Y.; Chen, X. A facile synthesis of highly luminescent nitrogen-doped graphene quantum dots for the detection of 2, 4, 6-trinitrophenol in aqueous solution. *Nanoscale* **2015**, *7*, 1872−1878.
(69) Wang, X.; Liu, Y.; Zhou, Q.; Sheng, X.; Sun, Y.; Zhou, B.; Zhao, J.; Guo, J. A reliable and facile fluorescent sensor from carbon dots for sensing 2, 4, 6-trinitrophenol based on inner filter effect. *Sci. Total Environ.* **2020**, *720*, 137680.

https://doi.org/10.1021/acsomega.1c03481
ACS Omega 2021, 6, 23475−23484